

1 **NO₂ seasonal evolution in the North Subtropical free** 2 **troposphere**

3

4 **M. Gil-Ojeda¹, M. Navarro-Comas¹, L. Gómez-Martín¹, J.A. Adame¹, A. Saiz-**
5 **Lopez², C. A. Cuevas², Y. González³, O. Puentedura¹, E. Cuevas³, J-F Lamarque⁴,**
6 **D. Kinninson⁴ and S. Tilmes⁴**

7 [1]{Instituto Nacional de Técnica Aeroespacial, Torrejón de Ardoz, Spain}

8 [2]{Atmospheric Chemistry and Climate Group, Institute of Physical Chemistry Rocasolano,
9 CSIC, Madrid, Spain}

10 [3]{Izaña Atmospheric Research Center, AEMET, Tenerife, Spain}

11 [4]{Atmospheric Chemistry Division, NCAR, Boulder, CO, USA}

12 Correspondence to: M. Gil-Ojeda (gilm@inta.es)

13

14 **Abstract**

15 Three years of Multi-Axis Differential Optical Absorption Spectroscopy (MAXDOAS)
16 measurements (2011-2013) have been used for estimating the NO₂ mixing ratio along a
17 horizontal line of sight from the high mountain Subtropical observatory of Izaña, at 2370 m
18 a.s.l. (NDACC station, 28.3°N, 16.5°W). The method is based on horizontal path calculation
19 from the O₂-O₂ collisional complex at the 477 nm absorption band which is measured
20 simultaneously to the NO₂, and is applicable under low aerosols loading conditions.

21 The MAXDOAS technique, applied in horizontal mode in the free troposphere, minimizes the
22 impact of the NO₂ contamination resulting from the arrival of MBL airmasses from thermally
23 forced upwelling breeze during central hours of the day. Comparisons with in situ observations
24 show that during most of measuring period the MAXDOAS is insensitive or very little sensitive
25 to the upwelling breeze. Exceptions are found under pollution events during southern wind
26 conditions. On these occasions, evidence of fast efficient and irreversible transport from the
27 surface to the free troposphere is found.

28 Background NO₂ vmr, representative of the remote free troposphere, are in the range of 20-45
29 pptv. The observed seasonal evolution shows an annual wave where the peak is in phase with

1 the solar radiation. Model simulations with the chemistry-climate CAM-Chem model are in
2 good agreement with the NO₂ measurements, and are used to further investigate the possible
3 drivers of the NO₂ seasonality observed at Izaña.

4 5 **1 Introduction**

6 Nitrogen oxides play an important role in tropospheric chemistry as they control the O₃
7 photochemical catalytic production (Crutzen, 1979), the abundance of hydroxyl radicals, and
8 contribute to the nitrate aerosols formation. In a background unpolluted atmosphere where NO_x
9 concentrations are low, net ozone loss occurs during photochemically active periods (Liu et al.,
10 1983; Isaksen et al., 2005). NO_x abundance is highly variable since it is influenced by non-
11 steady natural and anthropogenic emissions and its global distribution is still uncertain. Free
12 Troposphere (FT) source inventories indicate that major production comes from lighting (2-16
13 Tg N yr⁻¹), followed by NH₃ oxidation (0.3-3 Tg N yr⁻¹), stratospheric intrusion (0.08-1 Tg N
14 yr⁻¹) and aircraft (0.6-0.7 Tg N yr⁻¹). Contribution from the boundary layer in remote regions is
15 rare (Bradshaw et al., 2000).

16 Information of surface NO_x on polluted areas is available due to extended governmental air
17 quality networks. During the last decade, satellite instruments have demonstrated capabilities
18 for successful retrieval of tropospheric NO₂ identifying enhanced concentrations over urban
19 and industrial areas in the boundary layer (Richter et al., 2005; Irie et al., 2005) and tracking
20 the temporal trends (Hilboll et al., 2013; Cuevas et al., 2014). However, direct NO₂
21 measurements in the background FT are scarce due to the requirement of observational
22 platforms above, typically 2000 m a.s.l., but also due to the low concentrations present at those
23 levels.

24 Airborne NO₂ measurements have been performed for decades (Ridley et al., 1988; Carroll et
25 al., 1990), however the need for very short response times at concentrations close to the
26 instrumental detection limit, make the FT observations a challenging task. Even though well
27 characterized aircraft instruments reach detection limits as low as 10 pptv (Heland et al., 2002),
28 few studies are reported in the literature. Measurements are generally collected during
29 individual field campaigns associated to specific targets such as chemistry missions or satellite
30 validations (Jacob et al., 2003; Bucsela et al., 2008; Boersma et al., 2008; Baidar et al., 2013;
31 Flynn et al., 2014). These time and space sparse data limit the study of seasonalities or trends
32 in the FT. Only recently, attempts to obtain global FT NO₂ abundances from satellite OMI

1 instrument has been performed for the first time (Choi et al., 2014) by using the cloud slicing
2 technique (Ziemke et al., 2001). The method is based on the comparison of cloud and cloudless
3 scenes to derive the FT mean concentrations. Results show that valuable information on NO₂
4 large scale phenomena can be derived on areas where clouds presence is frequent but does not
5 provide results in places such as East Atlantic subtropical latitudes where high pressures are
6 dominant features.

7 Instruments operating in the few high mountain stations existent around the world are the only
8 alternative to monitor NO₂ in the background FT. However, the in situ measurements are often
9 affected by the “upslope breeze effect” (Kleissl et al., 2007; Val Martin et al., 2008; Rodriguez
10 et al., 2009; Reidmiller et al., 2010; Cuevas et al., 2013). Radiative heating in the mountain
11 slopes result in air upwelling from the boundary layer contaminating the daytime measurements
12 by generally larger values over the polluted lower layers.

13 Recently, Gomez et al. (2014) have presented a simple method based on a Modified
14 Geometrical Approximation (MGA) to estimate trace gases concentrations at the level of the
15 Izaña Observatory from MAXDOAS measurements. The horizontal path length is obtained
16 from the oxygen collisional complex (O₄, hereafter) simultaneously measured with the tracer
17 under consideration (NO₂ and O₃). Gomez et al. examined a short summer period to
18 demonstrate the validity of the method. Here we apply the same technique to data covering 3
19 full years (2011-2013) to analyze the seasonal evolution of the NO₂ concentrations in volume
20 mixing ratio (vmr). MAXDOAS present two main advantages with respect to the in situ
21 instrument at this location, both related to the very long optical path of the measurements of
22 over 60 km. Firstly, it minimizes the potential contribution of NO₂ that may be upwelled from
23 the marine boundary layer (MBL). The breeze layer has a limited vertical extension and its
24 relative contribution to the MAXDOAS long path is small. On the contrary, Izaña in situ data
25 around noon are strongly influenced by the underlying polluted MBL (Puentedura et al., 2012;
26 Gomez et al., 2014). Secondly, due to the long light paths achieved by MAXDOAS in the FT,
27 very low concentrations, of few ppt, can be measured.

28 Section 2 presents the method, its limits and associated errors. In Sect. 3 the station and data
29 sets are depicted. Section 4 describes the method used for profiles retrieval. The description of
30 the chemical and back trajectories models is done in Sect. 5. Finally, Sects. 6 and 7 present the
31 results and discussion, and summary, respectively.

32

1 2 Instrument and methodology

2 In year 2010 the DOAS spectrometer, operating in zenith mode at that time, was upgraded for
3 MAXDOAS measurements. The spectrometer records the sky spectrum in the visible range at
4 a spectral resolution of 0.55 nm in 10 elevation angles from -1 to 90°, and 1° field of view
5 covering a full cycle in 20 min. The number of cycles per day ranges from 26 at winter solstice
6 to 38 in summer. NO₂ is evaluated in the 425-520 nm range in order to simultaneously retrieve
7 the O₄ from the 477 nm absorbing band. The scanning plane is on 0° azimuth (North) to
8 minimize the dependence of the path with the azimuth (Wittrock et al., 2004). The instrument
9 is part of the Network for the Detection of the Atmospheric Composition Change (NDACC)
10 and other settings are those recommended for DOAS type spectrometers. NO₂ at 294K
11 temperature from Vandaele et al. (1998) and O₄ from Hermans et al. (1990) cross sections have
12 been used. Details of the instrument, settings and operational mode can be found in Puentedura
13 et al. (2012) and Gomez et al. (2014).

14 The Modified Geometry Approximation (MGA) described in Gomez et al., (2014) has been
15 used for the data analysis. NO₂ vmr at the level of the station is obtained by dividing the
16 differential slant column density (DSCD) measured in the horizontal geometry by the horizontal
17 optical path. The DSCD is obtained by subtracting the measurement obtained at the zenith
18 (SZA=90°) from the measurement in the horizontal path. In a first approximation, the slant
19 paths contributions of 0 and 90° geometries cancel out and only the signal of the tracers present
20 in the horizontal path remains (see Gomez et al., 2014 for details). The method assumes a quasi-
21 Rayleigh atmosphere, i.e. very low Aerosol Optical Depth (AOD), and a single scattering before
22 the photon reaches the detector. The path is obtained from the O₄ horizontal column since the
23 amount of O₂ is known from the independent air pressure measurements. The path length is
24 then corrected to account for the differences in wavelengths between the O₄ and NO₂ analysis
25 ranges. In practice, the scattering of the zenith path does not take place near the instrument but
26 at a few km above the level of the station. The actual concentration of a measured species X at
27 the station level is given by:

$$X_{vmr} = \frac{X_{DSCD}}{\frac{O_{4DSCD}}{[O_4]_{surface}} \cdot f + c} \quad [1]$$

1

2 Where X_{DSCD} and O_{4DSCD} are the slant measured columns of the species X and O_4 , respectively.
3 $[O_4]_{surface}$ is the O_4 at the level of the station, f is the correction factor due to differences in
4 wavelength absorption ranges of the specie under study with respect to O_4 that can be computed
5 from a radiative transfer model (RTM) and c is the error of the approach. The latter is a factor
6 accounting for the dependence with the different vertical distributions of both species and
7 AMFs.

8

$$9 \quad c = h(Rg - R'g') \quad [2]$$

10

11 h is the effective scattering height of the vertical ray. R and R' are the ratio of the mean
12 concentration of the layer divided by the concentration at the level of the station of tracer X and
13 O_4 , respectively, and g and g' accounts for their AMF in the zenith geometry ($g = \text{AMF}(\text{SZA}) -$
14 1), where SZA stands for Solar Zenith Angle.

15 The effective scattering height is defined as

16

$$17 \quad h(z) = \sum_{surface}^{top} \left(\frac{I(z)}{\int_{surface}^{top} I(z).dz} .z \right) \quad [3]$$

18

19

$$20 \quad \text{where } \frac{I(z)}{\int_{surface}^{top} I(z).dz}$$

21

22 represents the normalized contribution of the ray scattered at each atmospheric layer to the
23 total flux at surface. From radiative transfer calculations it can be shown that the effective
24 scattering height ranges between 6.5 and 7.5 km above the station for solar zenith angle (SZA)
25 below 70° , which we estimate as the validity limit of the method.

26 Since both NO_2 and O_4 are analyzed in the same spectral range, the difference between the
27 weighted center of the range for NO_2 , i.e. the effective wavelength, and that of O_4 is small. The
28 value of f is of 0.9 for a near-Rayleigh atmosphere.

1 By using Eq. (2), the error introduced in NO₂ vmr due to the geometrical approximation, if
2 assuming a constant mixing ratio of both O₄ and NO₂ with height, is of 9.0 % at 70° SZA and
3 of 2.3% at 50°. Since the scattering heights and the air mass factors are well known, the data
4 can be corrected. The only uncertainty is due to the R value related to the vertical distribution
5 of NO₂ within the FT. However, aircraft measurements over the ocean far from large industrial
6 areas show that the tropospheric vertical distribution is nearly constant above the MBL (Bucsela
7 et al., 2008)

8 In the presence of moderate or high aerosols loading at the level of the observational point,
9 multiple scattering takes place and the method is no longer valid. Assuming that the aerosol
10 layer is a well mixed layer, we estimate the AOD=0.1 at 500 nm as a safe limit (Gomez et al.,
11 2014).

12 Since the path length is obtained from O₄ measurements, uncertainty in the magnitude of its
13 absolute cross section is an additional source of error. It has been reported that paths obtained
14 from O₄ are even larger than that RT computed for a Rayleigh atmosphere (Wagner et al., 2002)
15 when using the generally accepted cross-sections reported in literature (Greenblatt, 1990;
16 Hermans et al., 1999), suggesting that cross-section are underestimated. There is, however, no
17 agreement in the magnitude of the correct values. We performed direct Sun measurements on
18 a very clear morning (Aerosol Optical Density at 500 nm over the observatory = $0.007 \pm$
19 0.00077) at an O₄ effective temperature of 250 K, and compared the retrieved slants columns
20 with the ones calculated from the local radiosounding of the day (7 October, 2014) up to 30 km
21 and the tropical standard atmosphere from 30 km upwards. Results show an excellent agreement
22 with no difference at the error level when the retrieval includes O₄ cross-sections at two
23 temperatures (Fig. 1). In this exercise, the Thalman & Volkamer (2013) cross-sections at 203
24 and 293 K were used. When including only the room temperature cross-section in the retrieval,
25 the obtained O₄ is 3-5 % too large.

26 Our results agree with the very recent report by Spinei et al. (2014) who found a temperature
27 dependence of 9% for a variation of 44 K and no pressure dependence based on direct sun and
28 aircraft MAXDOAS measurements. The conclusion of their work is that no corrections need to
29 be made for effective temperatures near 275 K. Since the present method uses only the
30 horizontal path, the temperature along the path is nearly constant and the seasonal variability in
31 the subtropical FT is small. Air temperature at the level of Izaña ranges from 277 K in January-

1 February to 287 K in July-August. Consequently, no more than 2 % of error is expected due to
2 this effect.

3 Typical NO₂ SCD root mean square error of the fit for horizontal geometry is of 3×10^{14} molec
4 cm⁻². These errors represent 15–20 % of the typical differential SCD. A summary of the
5 analysis errors is shown in Table 1.

6

7 **3 The Izaña observatory and dataset**

8

9 Izaña (28.3°N, 16.5°W) is a well known GAW-NDACC station located at the top of the Izaña
10 mountain, one of the peaks of the great crater of the Teide volcano, at 2370 m a.s.l., in Tenerife
11 Island. The observatory and related meteorology has been extensively described in previous
12 publications (i.e. Rodriguez et al., 2009; Cuevas et al., 2013). It is representative of the FT at
13 night. During daytime it is frequently affected by anabatic winds resulting from heating of the
14 ground. This upslope breeze carries boundary layer air masses to the FT. The intensity of the
15 wind peaks near the local noon and can extend well into the afternoon. It can be indirectly
16 quantified using the measurements of water vapour on the station since air masses from below
17 carry high humidity to the height of the observatory. The measurements of in situ NO₂ are also
18 useful for this purpose, since the BL NO₂ concentrations in populated areas near the coast are
19 typically more than one order of magnitude larger than the background FT.

20 For the present work only the horizontal spectra are analyzed. If the SZA was lower than 10°,
21 then the 70° elevation spectrum was used as reference to avoid spectral distortions due to too
22 short integration times. In all other cases the reference was the zenith spectrum of the same
23 cycle.

24 Data from three complete years (2011-2013) have been used after screening for (a) NO₂ RMSE:
25 Fit error is limited to 2×10^{15} molec cm⁻² and a signal to noise ratio of 0.5, which is
26 approximately the detection limit of the instrument. (b) High SZA: Only data corresponding to
27 data below SZA 70° are used in the present analysis to limit the error in the path calculations.
28 (c) Aerosol loading: Measurements on days with Aerosol Optical Depth (AOD) at 500 nm over
29 0.1, were rejected. (d) Length of the path: Individual measurements with paths shorter than 30
30 km were also rejected (broken clouds or narrow dust layers might cause this effect). (e)
31 Unrealistic negative values appearing occasionally. Over 15.000 of data passed all filters for

1 the 3 years period (40% of all possible data).

2

3 **4 The Optimal Estimation Method**

4 The Optical Estimation Method (OEM) has been extensively used on last years to obtain NO₂
5 vertical profiles on moderate to high polluted environments. However, on free troposphere
6 background conditions, the concentrations are near the instrumental detection limit (10-100
7 pptv) and in these conditions the method provide unrealistic profiles. In this work we have used
8 it only to characterize the vertical distribution of the plume in a particular case study in which
9 a high NO₂ airmass arrived to the station. The mean AOD-500 nm on the studied day was of
10 only 0.02. **Under these conditions the impact of the aerosol loading in the retrieval is very low.**
11 **A test with and without aerosols yield mean differences of 1.6% in the retrieval for heights**
12 **between 1 and 5 km. Since uncertainties in the OEM method are larger than that value,** aerosols
13 have not been included in the analysis.

14 Given a set of measurements \mathbf{y} with the errors covariance \mathbf{S}_ϵ , the OEM (Rodgers, 2000) provides
15 the state vector \mathbf{x} that maximizes the probability that \mathbf{x} , containing the trace gas vertical
16 distribution, belongs to the interval $[\mathbf{x}, \mathbf{x}+d\mathbf{x}]$. Following OEM approach, the maximum a
17 posteriori solution $\hat{\mathbf{x}}$ is calculated as:

$$18 \hat{\mathbf{x}} = \mathbf{x}_a + \mathbf{S}_a \mathbf{K}^T (\mathbf{K} \mathbf{S}_a \mathbf{K}^T + \mathbf{S}_\epsilon)^{-1} (\mathbf{y} - \mathbf{K} \mathbf{x}_a) = \mathbf{x}_a + \mathbf{G}_y (\mathbf{y} - \mathbf{K} \mathbf{x}_a)$$

19 Where the weighting functions matrix \mathbf{K} express the sensitivity of the measurements to
20 variations in the trace gas profile (NO₂ in this case). In this work, \mathbf{K} is obtained with the
21 SPSSDISORT pseudo-spherical radiative transfer solver of the libRadtran software package
22 (Mayer and Kylling, 2005). The \mathbf{x}_a vector and \mathbf{S}_a matrix correspond to an a priori NO₂ profile
23 and its corresponding error covariance matrix, respectively.

24 The gain matrix \mathbf{G}_y , given by the following expression, quantifies the sensitivity of the retrieval
25 to the measurements:

$$26 \mathbf{G}_y = \mathbf{S}_a \mathbf{K}^T (\mathbf{K} \mathbf{S}_a \mathbf{K}^T + \mathbf{S}_\epsilon)^{-1}$$

27 The averaging kernel matrix \mathbf{A} , is then obtained as follows:

$$A = G_y K$$

1

2 **A** expresses the sensitivity of the retrieval to the true state, and it has an important role in the
 3 characterization of the retrieval. The retrieval at a given altitude is an average of the total profile
 4 weighted by the corresponding row of **A**, also known as Averaging Kernel function (AK). In
 5 general, the AKs are functions with a single peak in the appropriate level, where the
 6 measurement provides additional information to add to the a priori profile. Trace of **A** provides
 7 the number of independent pieces that can be extracted from the retrieval, usually known as
 8 degrees of freedom (DFS). **Typical values of the DFS in our retrievals are around 1.8.**

9 Another parameter **determining** the quality of the retrievals is the total error of the state vector
 10 elements. This parameter is the addition of three contributions: (1) the smoothing of the true
 11 profiles given by **S_a**; (2) The systematic errors of the measurements, provided by **S_ε**; and (3)
 12 systematic errors of the forward model mainly provided by the uncertainties in the parameters
 13 characterizing the atmosphere. **Average total error (considering the three mentioned**
 14 **contributions) for all the considered profiles and altitudes ranging from 1 to 5 kms is 0.01 ppb.**
 15 The choose of the values corresponding to these three sources of error (**S_a**, **S_ε** and the
 16 atmosphere parameters) in our study will be described in the following paragraphs.

17 The NO₂ hourly profiles used as a priori profiles in our calculations were obtained using a
 18 photochemical box model (Denis et al., 2005) derived from the SLIMCAT 3-D chemical
 19 transport model (Chipperfield, 2006). Diagonal elements of **S_a** are usually chosen to be a
 20 percentage of **x_a**. In this case, following the L-curve method described in (Schofield, 2003),
 21 they have been set to 100% of **x_a**, and its non-diagonal elements are calculated as follows
 22 (Barret et al., 2002; Friess et al., 2006):

$$S_{aij} = \sqrt{S_{a_{ii}} S_{a_{jj}} \exp(-\ln 2) \left(\left(\frac{z_i - z_j}{\gamma} \right)^2 \right)}$$

23

24 Where **z_i** and **z_j** are the altitudes of the altitude grid levels **i** and **j** respectively, and **γ** is a half of
 25 the correlation length. The functions represented in the last equation are Gaussian correlation
 26 functions which account for correlations between trace gas concentrations at different altitudes.
 27 After several tests on the retrieval, **γ** value has been chosen to be 300 m, correspondings to the
 28 value (between 0.1 and 1 km) that maximizes the DFS (trace of **A**), for the overall retrieval as
 29 well as for the altitudes closer to the station (2.3-2.6 km).

1 In this work, y represents the differential slant column densities (DSCD) of NO_2 measured with
2 the MAX-DOAS spectrometer, and \mathbf{S}_ε is set to a diagonal matrix which diagonal elements
3 correspond to the molecular errors of the measurements.

4 Concerning parameters characterizing atmosphere in our calculations, vertical profiles of O_3 ,
5 O_2 , CO_2 and H_2O have been obtained from the standard atmosphere for tropical latitudes
6 (Anderson, 1986). Radio-sounding data performed the same day of our calculations provided
7 the pressure, temperature and air density vertical profiles used in our retrieval. We have
8 considered layers of 100 m from 0 to 10 km, and with the same width of those corresponding
9 to the standard atmosphere for tropical latitudes (Anderson, 1986) for altitudes over 10 km. In
10 this work, AKs are near zero for altitudes lower than 0.5 km and higher than 5 km (see Fig. 2).
11 The retrieved profiles have been obtained for altitudes up to 6 km.

12

13 **5 Model description and trajectory analysis**

14 CAM-Chem (Community Atmosphere Model with Chemistry) is a global 3D chemistry-
15 climate model fully integrated into the CESM framework (Community Earth System Model)
16 (Lamarque et al., 2012). In this work CAM-Chem has been configured using a horizontal grid
17 resolution of 1.91° latitude \times 2.5° longitude and 26 hybrid vertical levels from the surface to
18 approximately 38 km. All simulations have been performed in Specified dynamics (SD), using
19 offline meteorological fields to compute the atmospheric transport, considering the same high
20 frequency meteorological input from a previous CAM-Chem 15 years simulation. This implies
21 that the model is forced to evolve as if it were a Chemical Transport Model.

22 The model includes the tropospheric chemistry mechanism of MOZART-4, implementing also
23 organic and inorganic halogen (chlorine, bromine and iodine) photochemistry mechanism,
24 taking into account natural and anthropogenic sources, heterogeneous recycling and dry and
25 wet deposition (Saiz-Lopez et al., 2012; Ordoñez et al., 2012; Fernandez et al., 2014).
26 Anthropogenic emissions due to fossil fuel and biofuel combustions come from the POET
27 (Precursors of Ozone and their effects in the troposphere) database for 2000.

28 To investigate the air masses reaching the area of study, back trajectories were computed with
29 the HYSPLIT (Hybrid Single-Particle Lagrangian Integrated Trajectory) model, developed by
30 the NOAA's Air Resources Laboratory (ARL) (Draxler et al., 2009). The ECMWF (European
31 Centre for Medium Range Weather Forecasts) meteorological fields were used with a spatial
32 resolution of $0.25^\circ \times 0.25^\circ$, 22 vertical levels from the surface to 250 mb and a time resolution

1 of 6 h. Three-dimensional kinematic back trajectories were calculated. A daily back-trajectory
2 at 12:00 UTC, with a 168 h pathway (7 days) and at 2370 m a.s.l. was computed. Following the
3 HYSPLIT model tools back trajectories have been grouped in clusters (Stunder, 1996), arriving
4 at the Izaña observatory.

5

6 **6 Results and discussion**

7 **6.1 MAXDOAS vs. in situ**

8 Results of the NO₂ comparison can be classified according to three different meteorological
9 regimes. A period in 2013 has been selected to illustrate the differences in concentration
10 between the in situ local sampling and the MAXDOAS long-path average (Fig. 4, upper panel).
11 On days when the breeze is inhibited, the in situ data are representative of the FT, and the
12 agreement between instruments is very good (e.g. days 139-145). On days when anabatic winds
13 are present, NO₂ vmr increases are observed in the in situ measurements whereas MAXDOAS
14 signal remains at typical FT levels (e.g. days 130-137). Upslope winds cause an air mass
15 mixture with that associated by the FT synoptic wind. The upslope strength will depend
16 inversely on the intensity of the zonal synoptic winds. (Cuevas et al., 2013). In general, the
17 depth of the layer is not enough to contaminate the MAXDOAS path. This situation is the one
18 most commonly observed at Izaña. As expected, MAXDOAS provide a much better
19 representation of the FT background reactive gases. A third set of measurements is shown when
20 MAXDOAS data also suffer large increases (e.g. days 127-129). After excluding thunderstorms
21 with electric activity and wildfires in the area, it was found that this situation always takes place
22 in presence of southern winds. The only identified NO₂ large source upwind is the 980 MW
23 thermal power plant located 25 km south of Izaña, with a NO₂ emissions of 4.7×10^6 kg year⁻¹.
24 As previously reported (Persson and Grazzini, 2007), the thermal local circulations are not
25 captured by atmospheric global models even by the ECMWF 0.25° x 0.25° used in this study
26 which predicted trajectories above 2000 m all the way (Fig. 3, lower right). This orographically-
27 forced lifting mechanism has been found to be an efficient and fast way for irreversible transport
28 of surface air to the FT. Pollutants and minor gases of oceanic origin (i.e. IO, BrO) move
29 upslope crossing the MBL top in less than 1 h, and then are subsequently mixed with FT air.
30 The quantification of the amount of air mass transported from the lower layers of the MBL to
31 the FT is out of the scope of this work, but certainly data provide evidence for the existence of
32 an efficient and fast mechanism to supply halogens and other marine trace gases to the FT.

1 Since southern wind conditions are common during the summer months (50 % of the days) and
2 the mountain rift has a NE-SW orientation, and a length of about 30 km, the supply of marine
3 trace gases to the FT might be not negligible, at least on a local scale.

4 Surprisingly, the very high MAXDOAS vmr reach as much as a half of the levels observed by
5 the in situ sensor. This is related to the pointing direction of the DOAS spectrometer, since the
6 plume propagates northward, along the same direction of the spectrometer line of sight. The
7 path within the plume results in an enhancement of the absorption signal. Figure 4 shows the
8 NO₂ vmr vertical cross sections for the day 128/2013, obtained by using the OEM technique,
9 indicating that the enhancement takes place near the level of the station, with an upper limit
10 around 4 km. This confirms that once the air mass passes over the mountain obstacle it either
11 moves horizontally or descends again but remaining in the FT. Note that the instrument
12 scanning lowest angle is below the horizon (IEA = -1°), thus containing information about the
13 trace gas concentration below the station.

14 It is worth to mention that Southern winds are generally related to African air masses containing
15 Saharan dust and, as previously mentioned, those dusty days were filtered out from the analysis.
16 The only non-dusty south wind cases observed are from Atlantic air masses which suffered an
17 abrupt change in direction when approaching to Africa. Consequently the impact of this effect
18 on the overall dataset is small. Only five clear cases have been identified within the 3-year
19 record. Those cases have been removed for seasonal evolution studies.

20 Figure 4 (top panel) shows the NO₂ vmr seasonal evolution separated by year. The seasonal
21 behavior is similar in all three years, with the maximum in the summer months and the
22 minimum in winter time. Summer gaps result from the large number of Saharan dust intrusions
23 during these months. To explore a possible dependence of the retrieved concentrations with the
24 SZA, the data have been plotted in colors according the SZA (Fig. 5, mid panel). The maxima
25 in summer months are observed regardless the SZA excluding the possibility of stratospheric
26 contamination or any other SZA dependent artifact. The magnitudes of the retrieved
27 concentration are also independent of the RMSE (Fig. 5, lower panel). Sporadic peaks over 100
28 pptv are observed with no increase in typical retrieval errors. The scattering along the day is
29 also large with standard deviations of 10-15 pptv.

30 Monthly means clearly show the rapid spring build-up and the autumn decay (Fig. 6). Mean
31 values range from 20 to 44 pptv throughout the year. A summer maximum has previously been
32 found in unpolluted continental China in the boundary layer as result of soil biogenic NO

1 emissions (Van der A et al., 2006, Qi et al., 2014). However, NO₂ in long paths over the Atlantic
2 FT cannot be explained in this way. The output of the CAM-Chem model for the location and
3 the level of the station show similar results. The agreement with observational data is
4 particularly good for the period November to February. The NO₂ summer build-up takes place
5 across the entire FT (not shown). The winter to summer ratio is largest in the middle troposphere
6 at 8 km height. The peak FT NO₂ values occurring in summer was previously observed by Val-
7 Martin et al (2008), who attributed the summer maxima in NO₂ to North American biomass
8 burning during this season. The model results show no seasonal differences in the NO₂ chemical
9 formation/loss channels. However, an increase in the overall reactive nitrogen budget occurs in
10 this unpolluted FT site, as summer proceeds. We have explored two possibilities to explain the
11 seasonality of our observations:

12 **6.1.1 Contamination by anabatic winds**

13 It has been previously shown that MAXDOAS-MGA technique minimizes the unwanted effects
14 of MBL on FT measurements, but in principle, the influence of a potential seasonal cycle in the
15 intensity of the upwelling wind cannot be entirely ruled out. Since anabatic winds are driven
16 locally by surface heating, the depth of the layer of influence is expected to be of only a few
17 hundreds of meters but there is not enough information to quantify the size of this depth and
18 thus the potential contribution of a possible path contamination from air masses rich in NO₂
19 coming from below. Most of the works available in the literature refer to the BL, generally with
20 return flow back. However, cases of upwelling to the FT are reported as well. As early as 1923,
21 Wenger (1923) observed this situation at the slopes of the Teide mountain in Tenerife to up of
22 1500 m a.s.l. but no data were available above that height. In situ data in Fig. 1 show evidence
23 of MBL nitrogen oxides transported by anabatic winds up to the level of the station (2370 m
24 a.s.l.). However, an intensification of the upslope breeze in summer with respect to winter
25 would result in a larger vertical extension of the upwelling layer, increasing its relative
26 contribution in the MAXDOAS path. Out of the few large pollution cases, the concentrations
27 measured are too low for the OEM technique to be applied. It is nevertheless unlikely that the
28 summer increase in upwelling can account for the twofold increase in the background NO₂ vmr.
29 For instance, for a layer of 200 m with a NO₂ load of as high as 600 ppt would represent an
30 increase in the column of some 5-10 % of the background concentration for a clean day.

31 We have recalculated NO₂ monthly means only from the first morning data, namely data
32 between SZA 70° a.m. and 65° a.m. These SZA correspond to fractional days ranging from 0.42

1 in mid winter to 0.32 in summer. At this early time of day the anabatic wind is still under the
2 first stage of development and the intensity of the upwelling is of only a few percent of the
3 maximum value after noon. Results show that the seasonality in the SZA 65° to 70° data is
4 almost identical than that when considering data at all SZA (ratio >0.98). We therefore conclude
5 that the summer increase is not a result of the contamination by high NO₂ upwelled MBL air
6 masses.

7

8 **6.1.2 Changes in horizontal transport patterns along season**

9 Val-Martin et al. (2008) analysed NO₂ mountain data from Azores and reported larger summer
10 concentrations attributed to North American biomass burning. However, circulation at the
11 lower latitudes of Canary Island is quite different. Attempts to determine the global FT
12 distribution of NO₂, based on the cloud slicing technique, have recently been made with OMI
13 data (Choi et al, 2014), but the method does not provide results in summer over the Sahara
14 region due to lack of cloudiness.

15 HYSPLIT 7 days back trajectory cluster analysis shows that airmasses arriving to Izaña during
16 the reporting period are fundamentally of Atlantic origin, with a small portion arriving from
17 Africa during the summer period (Fig. 7), in agreement with the 22-year (1988-2009) backward
18 trajectory climatology reported by Cuevas et al. (2013). As previously mentioned, only NO₂
19 observations under no-dust conditions are considered, therefore days with African trajectories
20 are not included in the analysis. Winter trajectories are longer than the summer ones and 30%
21 of them cross the United States. All trajectory clusters show a steady descendent transport in
22 the last 96 hours prior to the arrival to Izaña and are originated at an altitude of 4000-5500 m
23 a.s.l.

24 The cluster analysis tells us that the origin of the NO₂ seasonal variation has to be searched in
25 the Western Atlantic area at much higher altitude than the station. The CAM-Chem model
26 sampled at the 5.9 km level shows larger summer values over North America and the
27 subtropical Atlantic, than in winter months, both in the range of the observed values (Fig. 8).
28 The phase of the mid-troposphere seasonal wave is opposite of the BL one (Lamsal et al., 2010)
29 and is probably due to a combination of seasonality in convection and lightning. Venting
30 processes from the BL to the FT over US has been studied (i.e. Parrish et al., 2004; Hudman
31 2007) finding export of NO_y, mainly in form of HNO₃ and PAN to the mid troposphere.
32 Convection is driven by surface insolation and has a clear seasonal wave. The same is true for

1 lightning since thunderstorms mainly occur during the spring-summer months.

2 Tropospheric vertical profiles (Fig. 9) show how NO₂ vmr are decreasing in wintertime from
3 the MBL to the mid FT whereas in summer the concentration remains constant up to 6 km and
4 then increases. At the 5 km level, the model shows differences from 15 to 40 pptv from winter
5 to summer. These calculated values are in agreement with the 40-50 pptv background NO₂ vmr
6 estimated by Choi et al., (2014) for the summer months FT in an extended area covering the
7 Western Atlantic from subtropics to mid latitudes.

8 The build-up is basically due to enhanced NO₂ formation via the NO+O₃ reaction under higher
9 concentration of NO as result of NO_y reconversion of PAN and HNO₃ in the FT. Note that the
10 lifetime of NO_y is long enough for NO_x-rich air masses, originated in North America, to reach
11 the African coast.

12 In summary, the NO₂ seasonal variation obtained from MAXDOAS measurements can be
13 explained with the help of the back trajectory cluster analysis and a chemistry-climate model
14 and result from a mixed effect of long-range transport and free tropospheric subsidence. This
15 is basically the same conceptual model that explains the origin or relatively high ozone values
16 recorded at Izaña in summertime described by Cuevas et al. (2013). The origin of the high
17 summer NO₂ values at Izaña is related to the larger background NO₂ vmr found over North
18 America in the mid FT, confirming earlier findings from Schultz et al. (1998).

19

20 **7 Summary**

21 NO₂ volume mixing ratio at the level of the high mountain observatory of Izaña (2370 m a.s.l.)
22 has been obtained for 3 years of data using the MAXDOAS technique and the recently reported
23 Modified Geometrical Approximation (MGA). The method uses the absorption of the O₂-O₂
24 collisional complex at 477 nm to obtain the horizontal path and is applicable in a near-Rayleigh
25 atmosphere. Only data from airmasses of aerosol optical depths below 0.1 were considered,
26 thus removing African airmasses loaded with Saharan dust. Results show that on most of the
27 observation days, data are representative of the free troposphere. Exceptions are found when
28 wind blows from the South. On these occasions, we find evidence that orographically forced
29 surface airmasses ascend upslope to the Izaña observatory providing a channel for irreversible
30 transport of surface origin species to the free troposphere and might provide an explanation for
31 the concentrations of halogens oxides found in this region.

1 The NO₂ seasonal evolution shows a well defined annual cycle in phase with solar radiation.
2 Mean mixing ratios ranges from 20 pptv in mid winter to 42 pptv in summer with a significant
3 day to day variability. By contrast, we find a small interannual variability during the 3-year
4 observation period. A number of possible causes to explain the observed seasonality have been
5 discussed including seasonal changes in transport and contamination due to seasonality in the
6 upslope winds (anabatic winds) but they individually could not provide an explanation of the
7 observations. CAM-Chem climate chemistry model reproduces the monthly distribution with
8 great accuracy. The results of the back trajectory cluster together with the model analysis show
9 that the seasonality in NO₂ vmr is related to a combined effect of long-range transport and
10 subsidence in the free troposphere. Dust-free trajectories follow North America/North Atlantic
11 pathways with airmasses coming from the mid-free troposphere, between 4000 and 5500 m
12 a.s.l. The model and previous satellite estimations show a seasonality in NO_y and NO₂ in the
13 mid free troposphere in phase with the MAXDOAS observations at Izaña. Larger summer
14 values are probably due to a combination of seasonality in convection and lightning.

15

16 **Acknowledgements**

17 This work was funded by the Spanish National R+D Funding Agency through project AMISOC
18 (CGL2011-24891) and the EU FP7 NORS project (Grant Agreement 284421). The authors
19 gratefully acknowledge NOAA Air Resources Laboratory for the provision of the HYSPLIT
20 transport and dispersion model.

21

1 **References**

- 2 Anderson, G. P.: AFGL atmospheric constituent profiles (0-120 km), Hanscom AFB, MA :
3 Optical Physics Division, Air Force Geophysics Laboratory, AFGL-TR ; 86-0110. U.S. Air
4 Force Geophysics Laboratory. Optical Physics Division, 1986.
- 5 Baidar, S., Oetjen, H., Coburn, S., Dix, B., Ortega, I., Sinreich, R., and Volkamer, R.: The CU
6 Airborne MAX-DOAS instrument: vertical profiling of aerosol extinction and trace gases,
7 *Atmos. Meas. Tech.*, 6, 719–739, 2013.
- 8 Barret, B., De Maziere, M. D., and Demoulin, P.: Retrieval and characterization of ozone
9 profiles from solar infrared spectra at the Jung-fraujoch, *J. Geophys. Res.* 107(D24), 4788,
10 doi:10.1029/2001JD001298, 2002.
- 11 Bradshaw, J., Newell, R., Sandholm S., and Liu, S.: Observed distributions of nitrogen oxides
12 in the remote free troposphere from the NASA Global Tropospheric Experiment Programs,
13 *R. Geophysics*, 38, 1, 2000.
- 14 Bucsela, E. J., Perring, A. E., Cohen, R. C. Boersma, K. F., Celarier, E. A. Gleason, J. F.,
15 Wenig, M. O., Bertram, T. H., Wooldridge, P.J., Dirksen, R., and Veefkind, J. P.:
16 Comparison of tropospheric NO₂ from in situ aircraft measurements with near-real-time and
17 standard product data from OMI, *J. Geophys. Res.*, V 113, D16S31,
18 doi:10.1029/2007JD008838, 2008.
- 19 Carroll, M.A., Hastie, D.R., Ridley, B.A., Rodgers, M. O., Torres, A. L., Davis, D. D.,
20 Bradshaw, J. D. Sandholm, S. T., Schiff, H.I., Karecki, D. R., Harris, G. W. Mackay, G. I.,
21 Gregory, G. L., Condin, E. P., Trainer, M., Hübler, G., Montzka, D. D., Madronic, S., H.,
22 Albritton, D. L., Singh, H. B., Beck, S. M., Shipham, M.C. and Bachmeier, A. S. Aircraft
23 Measurements of NO_x over the Eastern Pacific and Continental United States and
24 Implications for Ozone Production, *J. Geophys. Res.* V95, D7, pp 10.205-10.233, 1990.
- 25 Chipperfield, M. P.: New version of the TOMCAT/SLIMCAT off-line chemical transport
26 model: Intercomparison of stratospheric tracer experiments, *Q. J. R. Meteorol. Soc.*, 132,
27 1179–1203, doi:10.1256/qj.05.51, 2006.
- 28 Choi, S., Joiner, J., Choi, Y., Duncan, B. N., Vasilkov, A., Krotkov, N., and Bucsela, E.: First
29 estimates of global free tropospheric NO₂ abundances derived using a cloud slicing
30 technique applied to satellite observations from the Aura Ozone Monitoring Instrument
31 (OMI), *Atmos. Chem. Phys.*, 14, 10565–10588, doi:10.5194/acp-14-10565-2014, 2014.

1 Clémer, K., Van Roozendael, M., Fayt, C., Hendrick, F., Hermans, C., Pinardi, G., Spurr, R.,
2 Wang, P., and De Mazière, M., Multiple wavelength retrieval of tropospheric aerosol optical
3 properties from MAXDOAS Measurements in Beijing, *Atmos. Meas. Tech.*, 3, 863–878,
4 doi:10.5194/amt-3-863-2010, 2010.

5 Cuevas, E., González, Y., Rodríguez, S., Guerra, J. C., Gómez-Peláez, A. J., Alonso-Pérez, S.,
6 Bustos, J., and Milford, C., Assessment of atmospheric processes driving ozone variations
7 in the subtropical North Atlantic free troposphere, *Atmos. Chem. Phys.*, 13, 1973-1998,
8 doi:10.5194/acp-13-1973-2013, 2013.

9 Cuevas, C., Notario, A., Adame, J.A., Hilboll, A., Richter, A., Burrows, J. P. and A. Saiz-
10 Lopez, Evolution of NO₂ levels in Spain from 1996 to 2012, *Scientific Reports*, 4, 5887;
11 DOI:10.1038/srep05887, 2014.

12 Denis, L., Roscoe, H. K., Chipperfield, M. P., Van Roozendael, M., and Goutail, F.: A new
13 software suite for NO₂ vertical profile retrieval from ground-based zenith-sky spectrometers,
14 *J. Quant. Spectrosc. Rad. Transf.*, 92, 321–333, doi:10.1016/j.jqsrt.2004.07.030, 2005.

15 Draxler, R.R., Stunder, B., Rolph, G., Taylor, A. 2009. HYSPLIT_4 User's Guide, via NOAA
16 ARL website. NOAA Air Resources Laboratory, Silver Spring, MD, December 1997 (last
17 access: May 19, 2015), revised January 2009.
18 http://www.arl.noaa.gov/documents/reports/hysplit_user_guide.pdf

19 Emmons, L. K., Walters, S., Hess, P. G., Lamarque, J.-F., Pfister, G. G., Fillmore, D., Granier,
20 C., Guenther, A., Kinnison, D., Laepple, T., Orlando, J., Tie, X., Tyndall, G., Wiedinmyer,
21 C., Baughcum, S. L. and Kloster, S.: Description and evaluation of the Model for Ozone and
22 Related chemical Tracers, version 4 (MOZART-4), *Geosci. Model Dev.*, 3(1), 43–67,
23 doi:10.5194/gmd-3-43-2010, 2010.

24 Fernandez, R. P., Salawitch, R. J., Kinnison, D. E., Lamarque, J.-F. and Saiz-Lopez, A.:
25 Bromine partitioning in the tropical tropopause layer: implications for stratospheric
26 injection, *Atmos. Chem. Phys.*, 14, 13391-13410, doi:10.5194/acp-14-13391-2014, 2014.

27 Flynn, C. M., Pickering, K. E., Crawford, J. H., Lamsal, L. N., Krotkov, N. A., Herman, J.,
28 Weinheimer, A., Chen, G., Liu, X., Szykman, J., Tsay, S. C., Laughner, C. P., Hains, J., Lee,
29 P., Dickerson, R. R., Stehr, J. W., and Brent, L.: The relationship between column-density
30 and 20 surface mixing ratio: statistical analysis. *Atmos. Environ.* 92, 429-441, 2014.

1 Friess, U., Monks, P. S., Remedios, J. J., Rozanov, A., Sinreich, R., Wagner, T., and Platt, U.:
2 MAX-DOAS O₄ measurements: A new technique to derive information on atmospheric
3 aerosols: 2. Modeling studies, *J. Geophys. Res.*, 111, D14203, doi:10.1029/2005JD006618,
4 2006.

5 Gómez, L., Navarro-Comas, M., Puentedura, O., Gonzalez, Y., Cuevas, E. and Gil-Ojeda, M.:
6 Long-path averaged mixing ratios of O₃ and NO₂ in the free troposphere from mountain
7 MAX-DOAS *Atmos. Meas. Tech.*, 7, 1-12, 2014.

8 Granier, C., Guenther, A., Lamarque, J. F., Mieville, A., Muller, J., Olivier, J., Orlando, J.,
9 Peters, J., Petron, G., Tyndall, G., and Wallens, S.: POET, a database of surface emissions
10 of ozone precursors, available at at: <http://www.aero.jussieu.fr/projet/ACCENT/POET.php>
11 (last access: May 19, 2015), 2005.

12 Heland, J, Schlanger, H., Richter A., and Burrows, J.P.: First comparison of tropospheric NO₂
13 column densities retrieved from GOME measurements and in situ aircraft profile
14 measurements, *Geophys. Res. Lett.*, V29, N20, 1983, doi:10.1029/2002GL015528, 2002.

15 Hermans C., O₄ absorption cross-sections at 298K (335.59-666.63 nm), available at:
16 <http://spectrolab.aeronomie.be/index.htm> (last access: May 19, 2015), 2011.

17 Hilboll, A., Richter A., and Burrows, J. P.: Long-Term changes of tropospheric NO₂ over
18 megacities derived from multiple satellite instruments, *Atmos. Chem. Phys.*, 13, 4145–4169,
19 2013.

20 Hudman, R. C., Jacob, D. J., Turquety, S., Leibensperger, E. M., Murray, L. T., Wu, S.,
21 Gilliland, A. B., Avery, M., Bertram, T. H., Brune, W., Cohen, R. C., Dibb, J. E., Flocke, F.
22 M., Fried, A., Holloway, J, Neuman, J. A., Orville, R., Perring, A., Ren, X., Sachse, G. W.,
23 Singh, H. B., Swanson A., and Wooldridge, P. J.: Surface and lightning sources of nitrogen
24 oxides over the United States: Magnitudes, chemical evolution, and outflow, *J. Geophys.*
25 *Res.*, 112, D12S05, doi:10.1029/2006JD007912, 2007.

26 Irie, H., Sudo, K., Akimoto, H., Richter, A. Burrows, J. P., Wagner, T., Wenig, M., Beirle, S.
27 Kondo, Y., Sinyakov V. P. and Goutail, F.: Evaluation of long-term tropospheric NO₂ data
28 obtained by GOME over East Asia in 1996-2002, *Geophys. Res. Lett.*, V32, L11810,
29 doi:10.1029/2005GL022770, 2005.

30 Jacob, D.J., Crawford, J. H., Kleb, M- M., Connors, V. S., Bendura, R. J., Raper, J. L., Sachse,
31 G. W., Gille, J. G., Emmons, L., and Heald, C. L.: Transport and Chemical Evolution over

1 the Pacific (TRACE-P) aircraft mission: Design, execution, and first results, *J. Geophys.*
2 *Res.*, V 108, NO. D20, 9000, doi:10.1029/2002JD003276, 2003.

3 Kleissl, J. K., Honrath, R. E., Dziobak, M. P., Tanner, D., Val Martín, M., Owen, R. C. and
4 Helmig, C.: The occurrence of upslope flows at the Pico mountain top observatory: A case
5 study of orographic flows on a small, volcanic island, *J. Geophys. Res.*, 112, D10S35,
6 doi:10.1029/2006JD007565, 2007.

7 Lamarque, J.-F., Emmons, L. K., Hess, P. G., Kinnison, D. E., Tilmes, S., Vitt, F., Heald, C.
8 L., Holland, E. A., Lauritzen, P. H., Neu, J., Orlando, J. J., Rasch, P. J. and Tyndall, G. K.:
9 CAM-chem: description and evaluation of interactive atmospheric chemistry in the
10 Community Earth System Model, *Geosci. Model Dev.*, 5(2), 369–411, doi:10.5194/gmd-5-
11 369-2012, 2012.

12 Lamsal R. N., Martin, R. V., van Donkelaar, A., Celarier, E. A., Bucsela, E. J., Boersma, K. F.,
13 Dirksen, R., Luo, C. and Wang, Y.: Indirect validation of tropospheric nitrogen dioxide
14 retrieved from the OMI satellite instrument: Insight into the seasonal variation of nitrogen
15 oxides at northern midlatitudes. *J. of Geophys. Res.*, V. 115, D05302,
16 doi:10.1029/2009JD013351, 2010.

17 Mayer, B. and Kylling, A.: Technical note: The LibRadtran software package for radiative
18 transfer calculations – description and examples of use, *Atmos. Chem. Phys.*, 5, 1855–1877,
19 doi:10.5194/acp-5-1855-2005, 2005.

20 Ordóñez, C., Lamarque, J.-F., Tilmes, S., Kinnison, D. E., Atlas, E. L., Blake, D. R., Sousa
21 Santos, G., Brasseur, G. and Saiz-Lopez, A.: Bromine and iodine chemistry in a global
22 chemistry-climate model: description and evaluation of very short-lived oceanic sources,
23 *Atmos. Chem. Phys.*, 12(3), 1423–1447, doi:10.5194/acp-12-1423-2012, 2012.

24 Parrish D. D., Ryerson, T. B., Holloway, J. S., Neuman, J. A., Roberts, J. M., Williams, J.,
25 Stroud, C. A., Frost, G. J., Trainer, M., Hübler, G., Fehsenfeld, F. C., Flocke F., and
26 Weinheimer, A. J.: Fraction and composition of NO_y transported in air masses lofted from
27 the North American continental boundary layer, *J. Geophys. Res.*, V109, D09302, DOI:
28 10.1029/2003JD004226, 2004.

29 Parrish D. D., Ryerson, T. B., Holloway, J. S., Neuman, J. A., Roberts, J. M., Williams, J.,
30 Stroud, C. A., Frost, G. J., Trainer, M., Hübler, G., Fehsenfeld, F. C., Flocke F., and
31 Weinheimer, A. J.: Fraction and composition of NO_y transported in air masses lofted from

- 1 the North American continental boundary layer, *J. Geophys. Res.*
2 DOI: 10.1029/2003JD004226, 2004.
- 3 Persson, A. and Grazzini, F., User Guide to ECMWF forecast products, *Meteorological Bulletin*
4 M3.2, Edited by ECMWF. Available at:
5 http://www.uio.no/studier/emner/matnat/geofag/GEF4220/v09/undervisningsmateriale/Persson_user_guide.pdf (last access May 19, 2015), Updated 2007.
6
- 7 Puentedura, O., Gil, M., Saiz-Lopez, A., Hay, T., Navarro-Comas, M., Gomez-Pelaez, A.,
8 Cuevas, E., Iglesias J., and Gomez, L.: Iodine monoxide in the North subtropical free
9 troposphere, *Atmos. Chem. Phys.*, 12, 4909–4921, doi:10.5194/acp-12-4909-2012, 2012.
- 10 Qi, Y.: Spatio-Temporal distributions of tropospheric NO₂ over Oases in Taklimakan Desert,
11 China, *Chin. Geogra. Sci.*, 1-8, doi:10.1007/s11769-014-0696-z, 2014.
- 12 Reidmiller D.R., Jaffee, D. A., Fischer E. V., and Finley, B.: Nitrogen oxides in the boundary
13 layer and free troposphere at the Mt. Bachelor Observatory, *Atmos. Chem Phys.*, 10, 6043-
14 6062, 2010.
- 15 Richter, A., Burrows, J. P., Nüs, H., Granier C., and Niemeier, U.: Increase in tropospheric
16 nitrogen dioxide over China observed from space, *Nature* 437, 129-132,
17 doi:10.1038/nature04092, 2005.
- 18 Ridley, B. A., Carroll, M. A., Gregory, G. L., and Sachse, G. W.: NO and NO₂ in the
19 troposphere: Technique and measurements in regions of a folded tropopause *J. Geophys.*
20 *Res.*, 93, 15,813-15,830, 1988.
- 21 Rodgers, C. D.: *Inverse Methods for Atmospheric Sounding: Theory and Practice*, vol. 2 of
22 *Atmospheric, Oceanic and Planetary Physics*, World Scientific, Hackensack, NJ,
23 doi:10.1142/9789812813718_fmatter, 2000.
- 24 Rodriguez, S., Y. Gonzalez, E. Cuevas, R. Ramos, P. M. Romero, J. Abreu-Afonso and A.
25 Redondas, Atmospheric nanoparticle observations in the low free troposphere during
26 upward orographic flows at Izana Mountain Observatory *Atmos. Chem. Phys.*, 9, 6319–
27 6335, 2009.
- 28 Saiz-Lopez, A., Lamarque, J.-F., Kinnison, D. E., Tilmes, S., Ordóñez, C., Orlando, J. J.,
29 Conley, A. J., Plane, J. M. C., Mahajan, A. S., Sousa Santos, G., Atlas, E. L., Blake, D. R.,
30 Sander, S. P., Schauffler, S., Thompson, A. M. and Brasseur, G.: Estimating the climate

1 significance of halogen-driven ozone loss in the tropical marine troposphere, *Atmos. Chem.*
2 *Phys.*, 12(9), 3939–3949, doi:10.5194/acp-12-3939-2012, 2012.

3 Schultz, M., Schmitt, R., Thomas, K., Volz-Thomas, A., Photochemical box modeling of long-
4 range transport from North America to Tenerife during the North Atlantic Regional
5 Experiment (NARE) 1993, *J. Geophys. Res.* 103, D11, 13477–13488, DOI:
6 10.1029/97JD01481, 1998.

7 Spinei, E., Cede, A., Herman, J., Mount, G. H., Eloranta, E., Morley, B., Baidar, S., Dix, B.,
8 Ortega, I., Koenig, T. and Volkamer, R.: Direct sun and airborne MAX-DOAS
9 measurements of the collision induced oxygen complex, O₂-O₂ absorption with significant
10 pressure and temperature differences, *Atmos. Meas. Tech. Discuss.*, 7, 10015-10057, 2014.

11 Stunder, B. An assessment of the Quality of Forecast Trajectories. *Journal of Applied*
12 *Meteorology* 35, 1319-1331, 1996.

13 Thalman, R., and Volkamer, R. Temperature dependent absorption cross-sections of O₂-O₂
14 collision pairs between 340 and 630 nm and at atmospherically relevant pressure, *Phys Chem*
15 *Chem Phys.*, 15, doi: 10.1039/c3cp50968k, 2013.

16 Vandaele, A. C., Hermans, C., Simon, P. C., Carleer, M., Colins, R., Fally, S., Mérienne, M.
17 F., Jenouvrier, A., and Coquart, B.: Measurements of the NO₂ Absorption Cross-Sections
18 from 42000 cm⁻¹ to 10000 cm⁻¹ (238–1000 nm) at 220 K and 294 K, *J. Quant. Spectrosc.*
19 *Ra.*, 59, 171–184, doi:10.1016/S0022-4073(97)00168-4, 1998.

20 Val-Martin, M., Honrath, R. E., Owen, R. C., and Li, Q. B.: Seasonal variation of nitrogen
21 oxides in the central North Atlantic lower free troposphere *J. Geophys. Res.*, V113, D17307,
22 doi:10.1029/2007JD009688, 2008.

23 Van der A., R. J., Peters, D. H. M. U., Eskes, H., Boersma, K. F., Van Roozendaal, M., De
24 Smedt, I., and Kelder, H. M.: Detection of the trend and seasonal variation in tropospheric
25 NO₂ over China, *J. of Geophys. Res.*, V111, D12317, doi:10.1029/2005JD006594, 2006.

26 Wagner, T., Dix, B., Friedeburg, C.V., Friess, U., Sinreich, R., and Platt, U.: MAX-DOAS O₄
27 measurements: A new technique to derive information on atmospheric aerosols – Principles
28 and information content, *J. Geophys. Res.*, 109, D22205, doi:10- 1029/2004JD0044904,
29 2004.

- 1 Wagner, T., von Friedeburg, C., Wening, M., Otten, C., and Platt, U.: UV-Visible observations
2 of atmospheric O₄ absorptions using direct moonlight and zenith-scattered sunlight for clear
3 sky and cloudy sky conditions, *J. Geophys. Res.*, 107, 4424, doi:10.1029/2001JD001026,
4 2002.
- 5 Wenger, R. Zur Theorie der Berg- und Talwinde', *Meteorol. Zeits.* 7, 193–204, 1923.
- 6 Wittrock, F., Oetjen, H., Richter, A., Fietkau, S., Medeke, T., Rozanov, A., and Burrows, J. P.:
7 MAX-DOAS measurements of atmospheric trace gases in Ny-Alesund – Radiative transfer
8 studies and their application, *Atmos. Chem. Phys.*, 4, 955–966, doi:10.5194/acp-4-955-
9 2004, 2004.
- 10 Ziemke, J. R., Chandra, S., and Bhartia, P. K.: “Cloud slicing”: a new technique to derive upper
11 tropospheric ozone from satellite measurements, *J. Geophys. Res.*, 106, 9853–9867, 2001.
- 12 Zien, A.W., Reichter, A., Hillboll, A., Blechschmidt A.-M., and Burrows, J. P.: Systematic
13 analysis of tropospheric NO₂ long-range transport events detected in GOME-2 satellite data,
14 *Atmos. Chem Phys.*, 14, 7367-7396, doi:10.5194/acp-14-7367-2014, 2014.

1
2
3
4
5
6
7
8
9
10
11
12

Table 1. Method uncertainty

Uncertainty in NO ₂ due to fit	15-20%
Uncertainty in path due to the O ₄ fit	< 1%
Uncertainty of the method (related to unknown vertical distribution of NO ₂ and actual effective path)	2.5-9% (for sza: 50° to 70°)
Error in horizontal path due to O ₄ cross-sections temperature dependence	2%
OVERALL UNCERTAINTY	20-32%

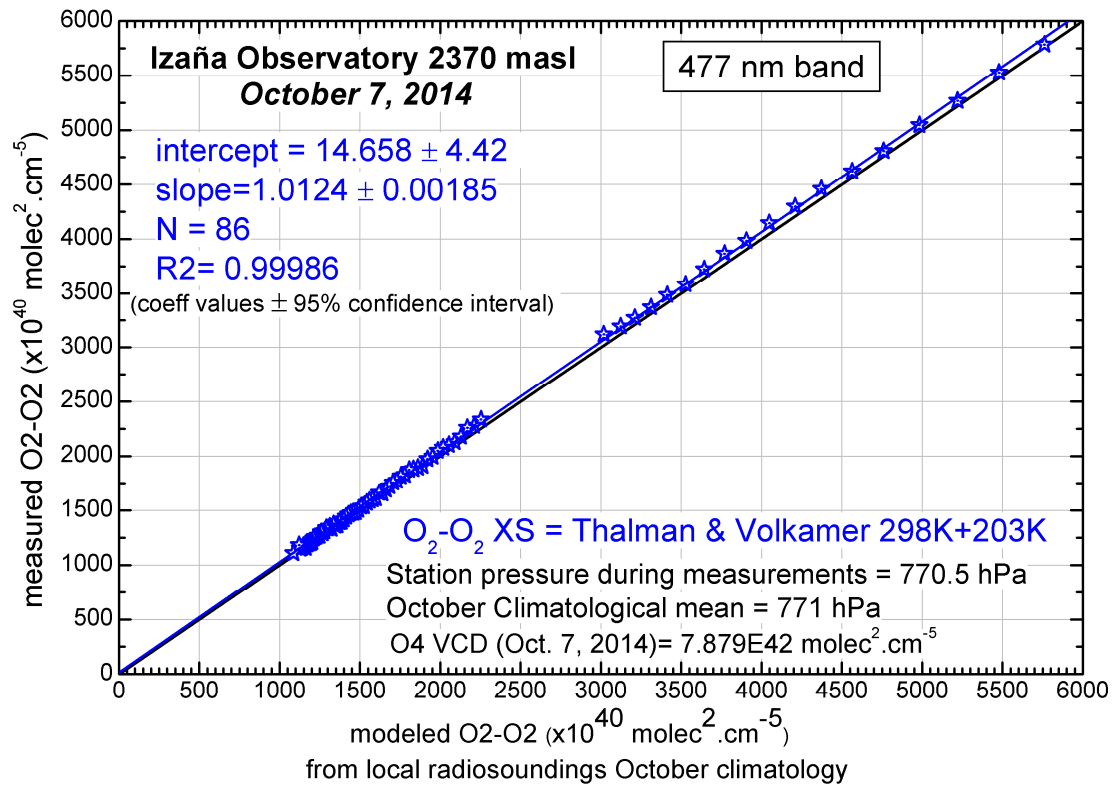
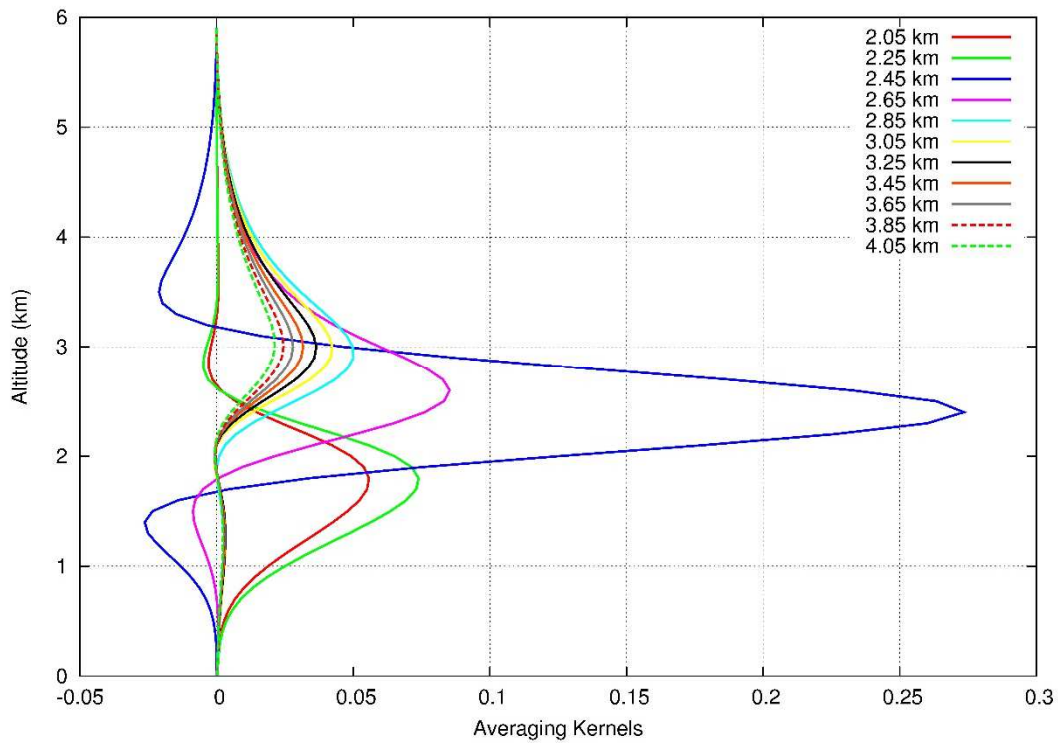
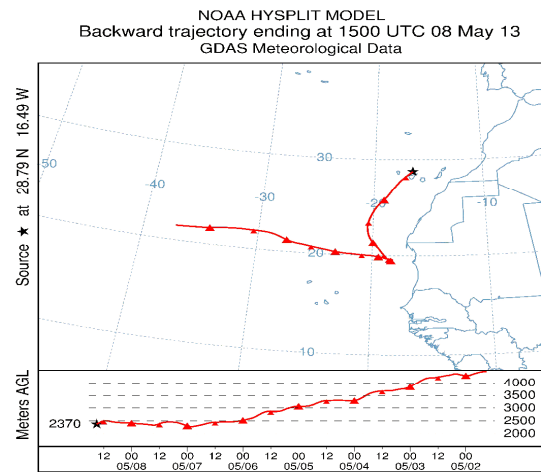
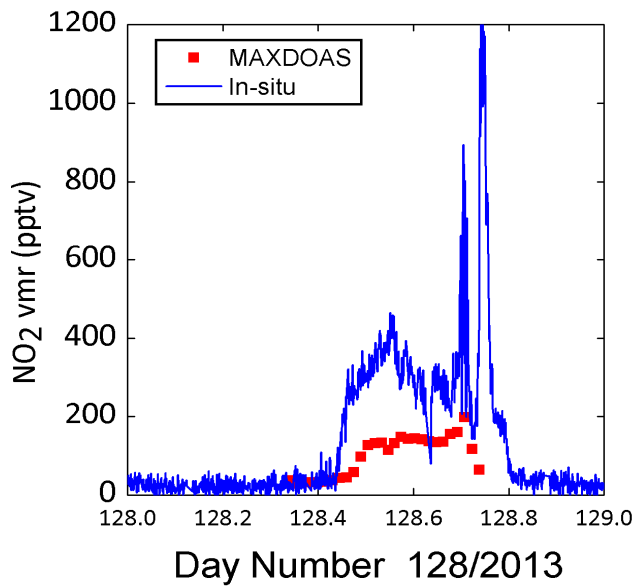
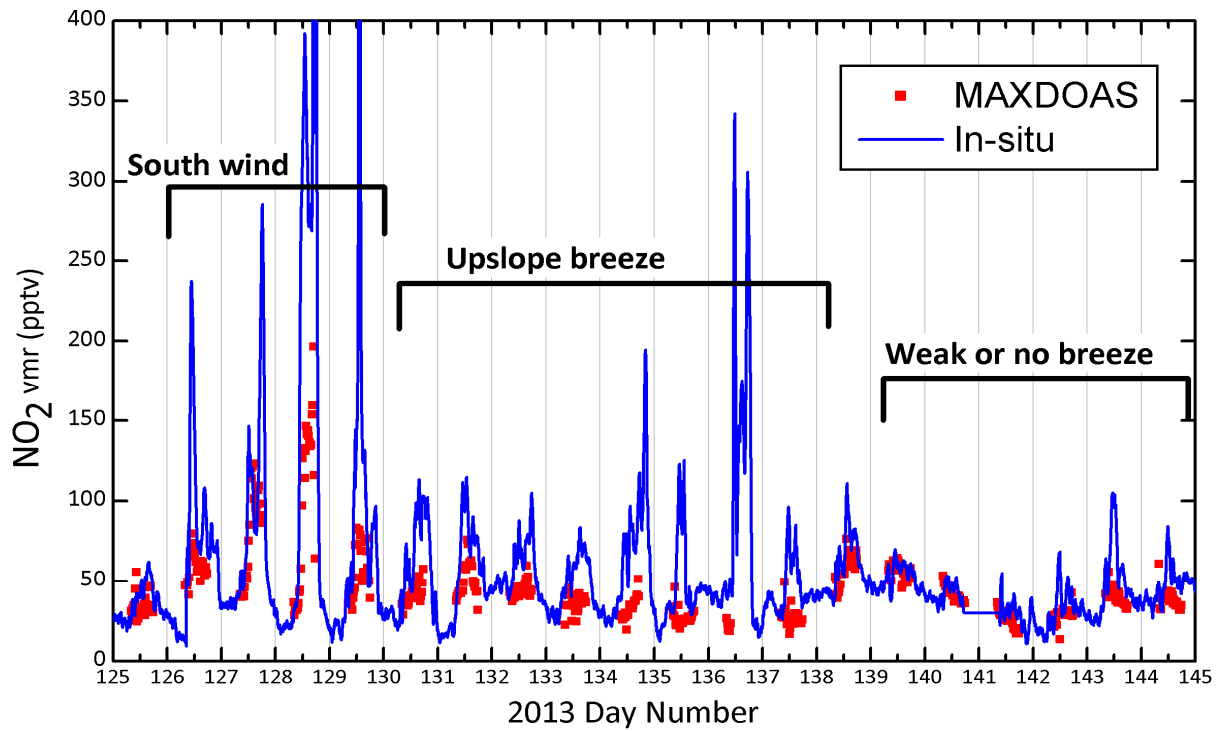


Figure 1. Measured O₄ SCD versus modeled O₄ for a pure Rayleigh atmosphere at the 477 nm band by using cross-sections at 203K and 293K temperatures (see text for details)



1
2
3
4
5

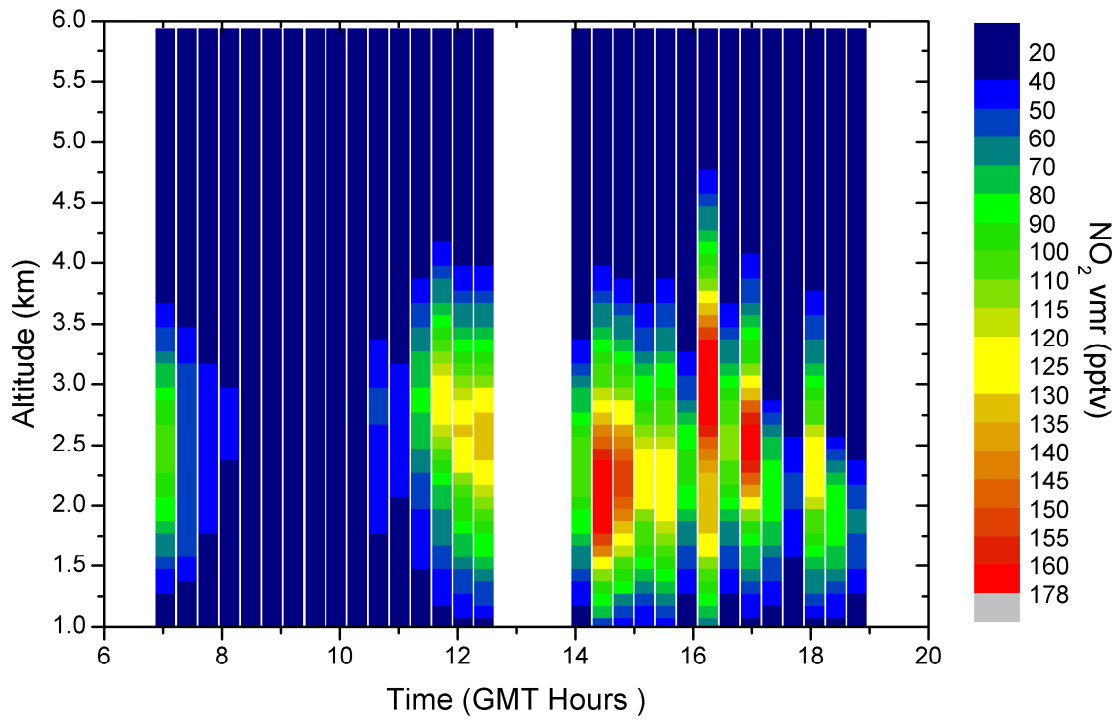
Figure 2 Example of NO₂ averaging kernels obtained in our profile retrieval corresponding to May 8th, 2013, at 12:00 UTC.



1

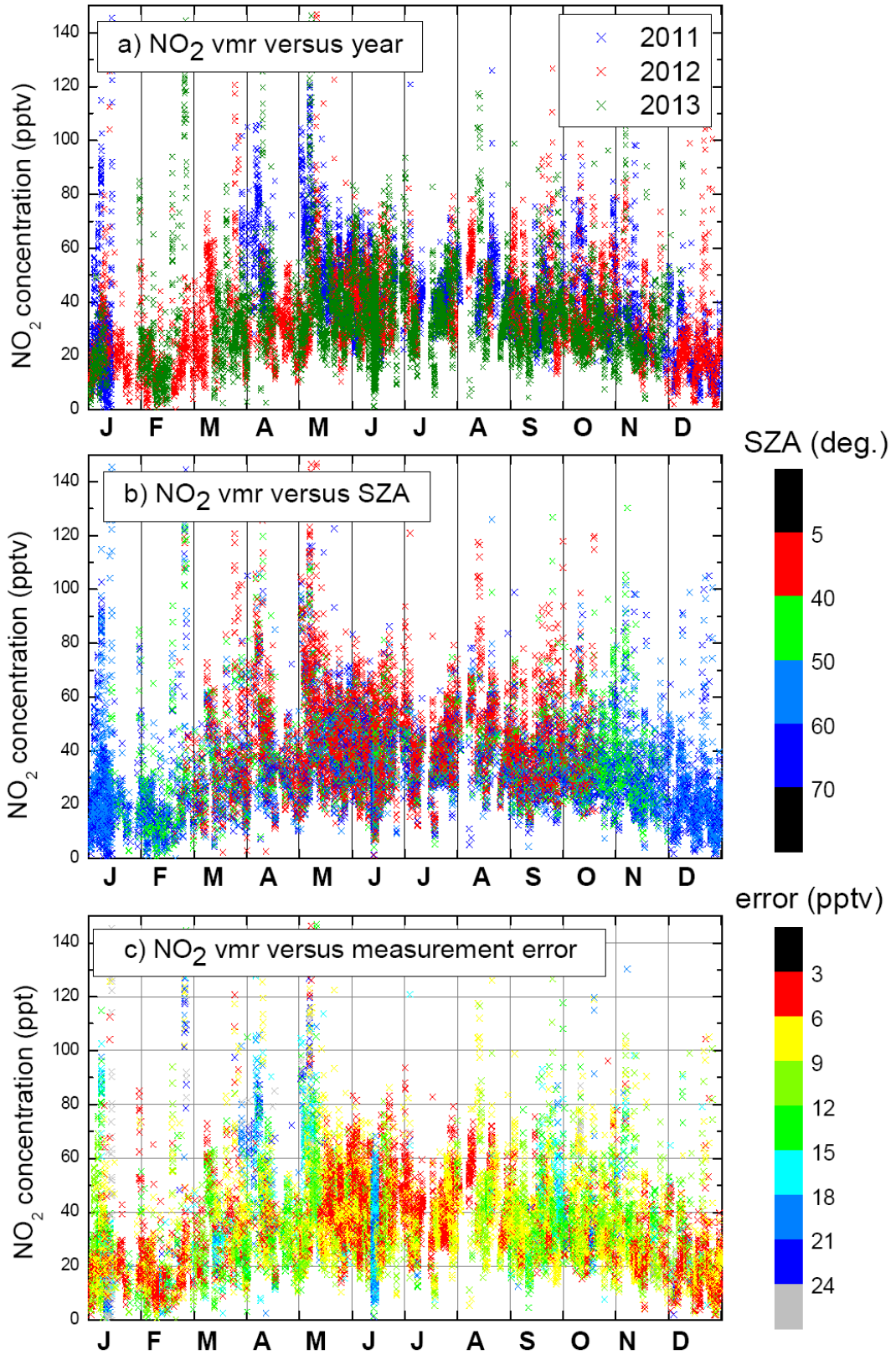
2 Figure 3. Izaña MAXDOAS versus minuted in-situ NO_2 volume mixing ratio for a period of
 3 time representative of 3 different wind situation. *In-situ* data are smoothed by 50-minutes
 4 running mean. (Top panel). Expanded plot for day May 8, 2013 (day number 128).
 5 Backtrajectory ending at Izaña at 15h of the same day.

6



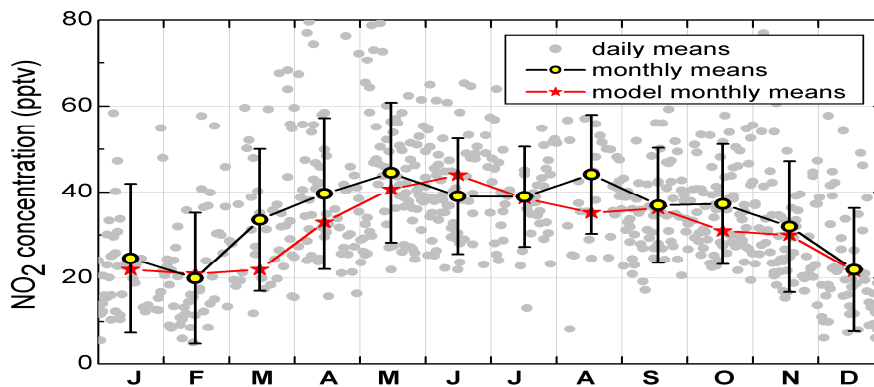
1
2
3
4
5

Figure 4. Unsmoothed vertical profiles of NO₂ vmr (in ppbv) for day 128/2013 obtained by OEM technique. Each vertical column represents an individual scanning cycle. (For details see [text](#))



1 Figure 5. Seasonal evolution of the individual data NO₂ vmr separated by years (Upper panel).
 2 Separated by Solar Zenith Angles (Mid panel) and separated by RMSE (Lower panel).

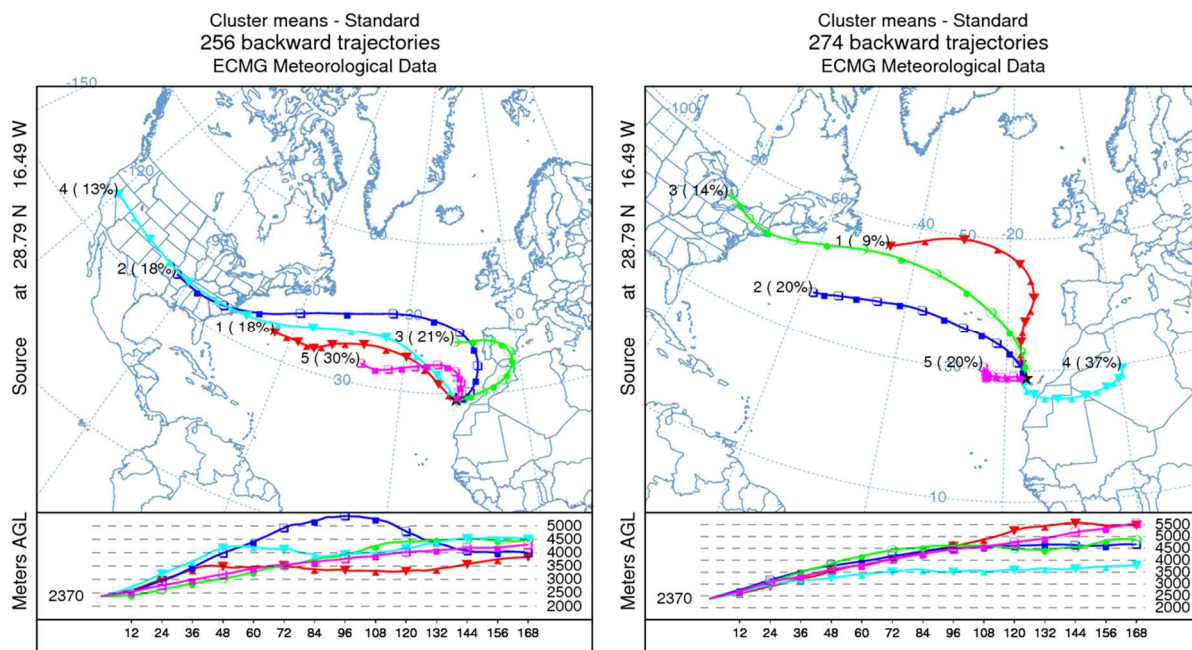
3



4

5 Figure 6. NO₂ concentration monthly means at the level of Izaña Observatory with their
 6 respective standard deviations (open circles and black lines). CAM-Chem model results for the
 7 same level are shown for comparison (Red stars and lines). Individual solid grey circles are the
 8 3-years diurnal mean

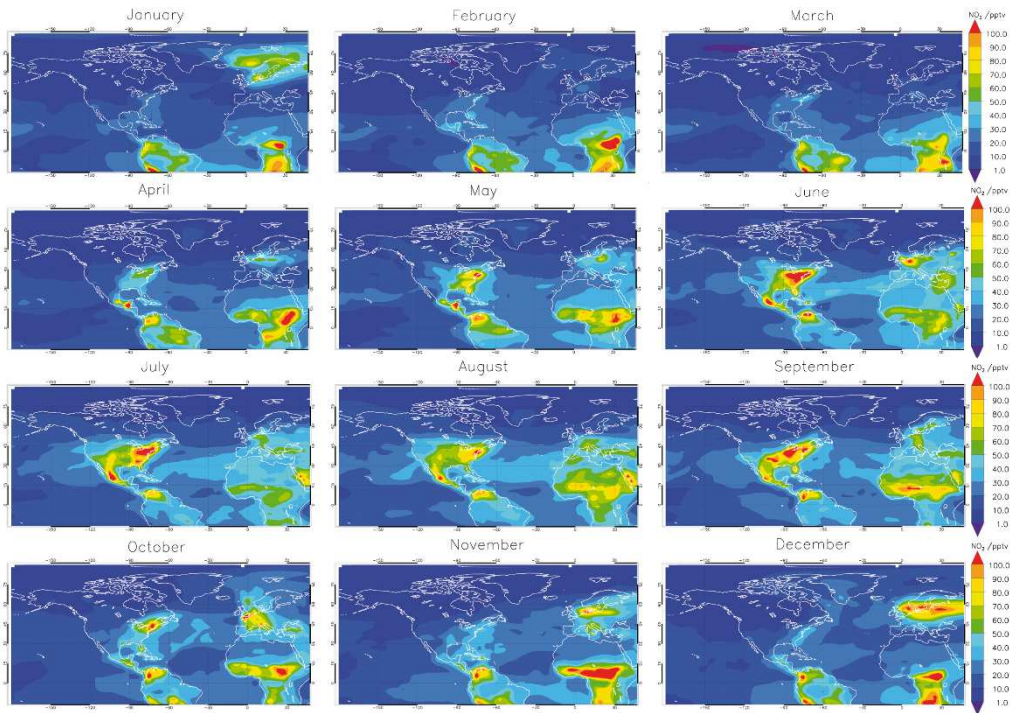
9



10

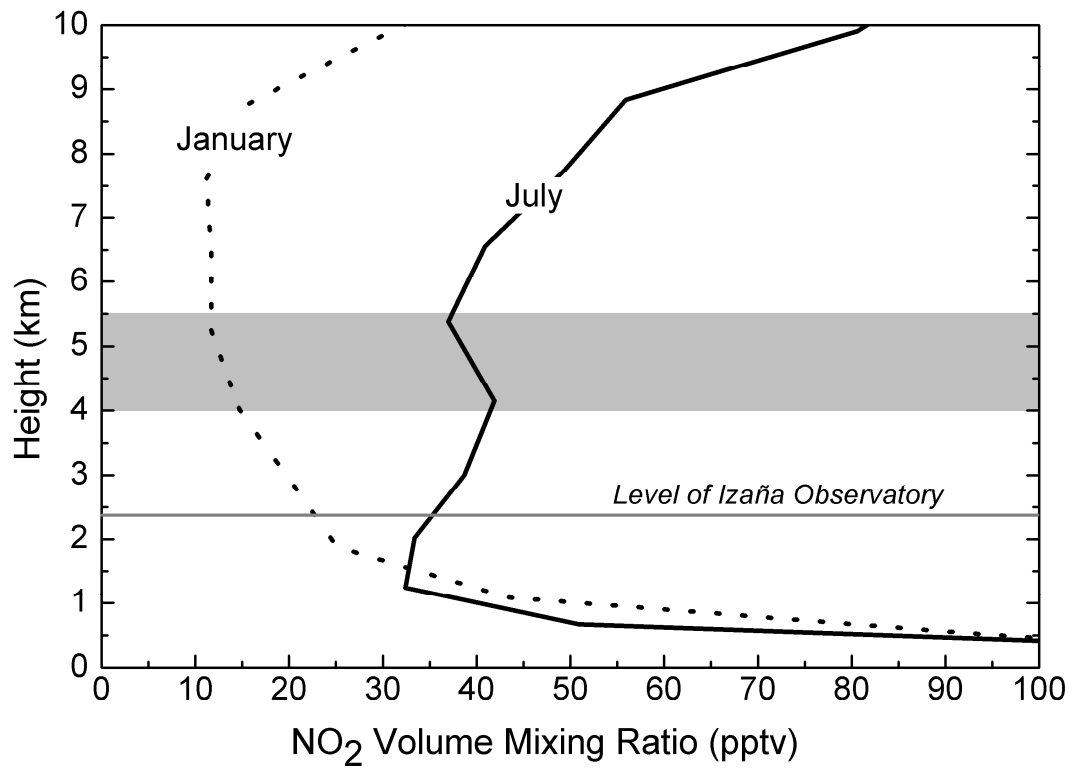
11 Figure 7. 1-week HYSPLIT back trajectories clusters arriving to Izaña Observatory for the left
 12 panel: winter months (DJF), right panel: summer months (JJA) and years 2011-2013

13



1

2 Figure 8. Global distributions of monthly mean NO_2 vmr for the level 5.9 km obtained from the
 3 Cam-CHEM chemistry climate model-model.



1

2 Figure 9. NO₂ vmr monthly means vertical profiles from Cam-CHEM model.

3 Gray band represents the height range where airmasses are originated (see text).